

Ratiometric Imaging of the T-cell actin cytoskeleton reveals the nature of receptor-induced cytoskeletal enrichment

Alexander A. Smoligovets,^{†‡§} Adam W. Smith,^{†¶} Jay T. Groves,^{†*}

[†]Howard Hughes Medical Institute, Department of Chemistry, University of California, Berkeley, California; [‡]Physical Biosciences and Materials Sciences Divisions, Lawrence Berkeley National Laboratory, Berkeley, California; [§]Department of Molecular and Cell Biology, University of California, Berkeley, California; [¶]Currently at the Department of Chemistry, University of Akron, Akron, Ohio

ABSTRACT The T-cell actin cytoskeleton mediates adaptive immune system responses to peptide antigens by physically directing the motion and clustering of T-cell receptors (TCRs) on the cell surface. When TCR movement is impeded by externally applied physical barriers, the actin network exhibits transient enrichment near the trapped receptors. The coordinated nature of the actin density fluctuations suggests that they are composed of filamentous actin, but it has not been possible to eliminate *de novo* polymerization at TCR-associated actin polymerizing factors as an alternative cause. Here, we use a dual-probe cytoskeleton labeling strategy to distinguish between stable and polymerizing pools of actin. Our results suggest that TCR-associated actin consists of a relatively high proportion of the stable cytoskeletal fraction and extends away from the cell membrane into the cell. This implies that actin enrichment at mechanically trapped TCRs results from three-dimensional bunching of the existing filamentous actin network.

The T-cell actin cytoskeleton is critical for proper antigen recognition by the mammalian adaptive immune system. During T-cell receptor (TCR) triggering by antigen peptides presented on major histocompatibility proteins (pMHCs) on the surfaces of antigen-presenting cells (APCs), the T-cell actin cytoskeleton adopts a pattern of centrosymmetric retrograde flow (1–3). This simultaneously promotes further TCR triggering (4) and rearranges various T-cell membrane proteins and their APC counterparts into an organized cell-cell interface termed the immunological synapse (IS) (5–7). During this process, TCRs form microclusters that move to the center of the IS in an actin-dependent manner (8, 9). When engineered physical barriers interrupt the centripetal motion of TCR clusters, actin flow slows near the pinned microclusters, and the cytoskeletal network transiently accumulates and dissipates at the sites (10, 11). The amplitude and duration of the induced cytoskeletal fluctuations are much greater than would be expected for a random distribution of independent objects, indicating that the actin in the local environment is coordinated. Whether this coordination arises from a rearrangement in the existing F-actin network or represents *de novo* polymerization of the cytoskeleton, as predicted by the association of TCRs with actin polymerizing factors (12), remains unclear. Here, we use a dual-probe cytoskeleton labeling approach that has previously been applied to distinguish between stable and dynamic populations of actin by exploiting the different relative affinities of monomeric actin and actin-binding proteins towards each population (13). This strategy reveals that TCR-associated actin is composed primarily of the stable cytoskeletal fraction and that local enrichment results from three-dimensional bunching of the existing filamentous actin network.

Primary T cells from mice transgenic for the AND TCR were triggered using synthetic APCs consisting of supported lipid bilayers functionalized with pMHC and the integrin ligand intercellular adhesion molecule 1 (ICAM-1). Nanopatterned metal grids on the bilayer substrate acted as diffusion barriers that prevented lateral transport of TCR-pMHC complexes (14, 15). Transient enrichment of actin at TCR clusters trapped at these barriers was visualized using fluorescent fusions of actin itself (mKate2- β -actin) and the F-actin binding domain of utrophin (EGFP-UtrCH). Such a dual-probe strategy theoretically allows for discrimination between different pools of actin: dynamic populations characterized by high polymerization and/or short filament fragments tend to be relatively better labeled by direct actin fusions whereas stable populations composed of longer filaments can support higher labeling by fluorescent fusions of F-actin binding proteins. This visualization method has been validated in *Xenopus* oocytes, where it distinguishes actin populations during wound healing (13). It has not been explicitly applied to T cells; however, simultaneous labeling of the Jurkat cell cytoskeleton using EGFP-actin and Alexa 568-phalloidin reveals distinct populations of actin consistent with the results expected from *Xenopus* (13, 16).

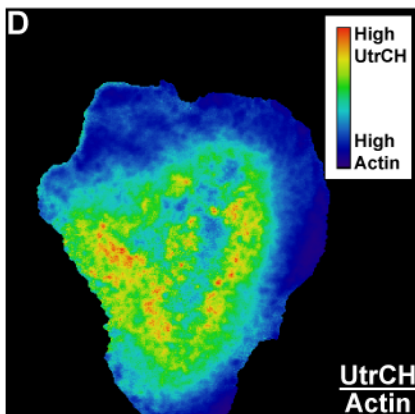
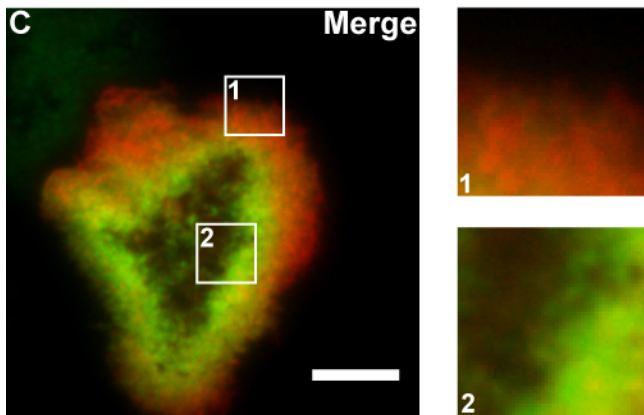
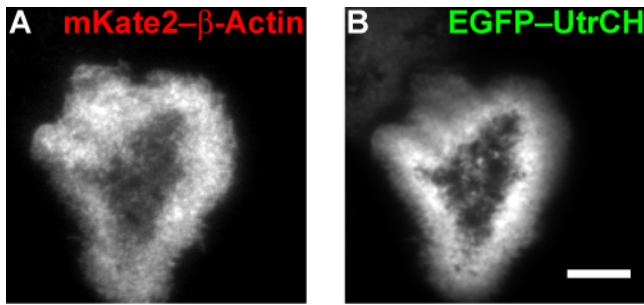


Figure 1. Ratiometric imaging of the cytoskeleton in live T cells distinguishes between dynamic and stable actin populations. (A) mKate2- β -actin, (B) EGFP-UtrCH, and (C) merged images of a triggered T cell show different actin pools. The cutouts in (C) correspond to a region high in dynamic actin featuring short, polymerizing filaments and/or actin monomers (1) and a region with a stable actin population featuring longer filaments to which UtrCH can bind (2). (D) The UtrCH/actin ratio image highlights pools of relatively high UtrCH (red) or actin (blue). (Scale bars: 5 μ m.)

network (3, 16). An effective way to highlight each of these cytoskeletal regions is to consider the relative ratios of the two probes at each location. In this case, a high UtrCH/actin ratio corresponds to stable actin, and a high actin/UtrCH ratio corresponds to dynamic actin (Fig. 1 D). When T cells are treated with cytochalasin D, an inhibitor of actin polymerization, the overall UtrCH/actin ratio of the cell decreases as would be expected from a general decrease in polymerized actin (Movies S7 and S8 in the Supporting Material). However, it should be noted that photobleaching can also shift the UtrCH/actin ratio over time.

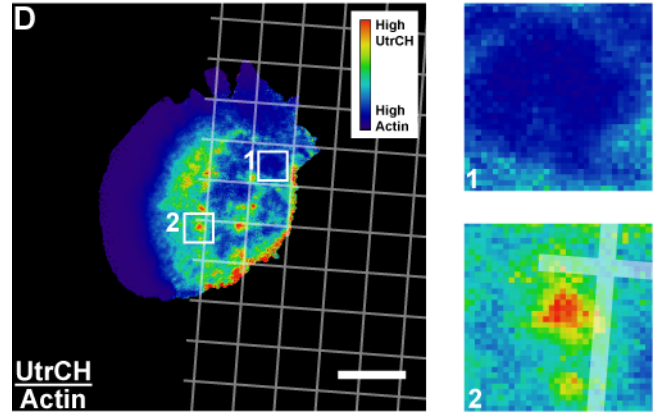
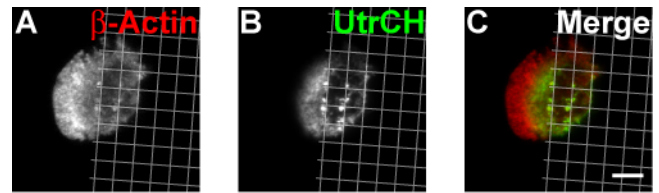


Figure 2. Receptor-induced cytoskeletal enrichment at sites of pinned TCRs corresponds to a primarily stable actin fraction. (A) mKate2- β -actin, (B) EGFP-UtrCH, and (C) merged images of a triggered T cell interacting with a nanopatterned supported lipid bilayer show actin enrichment corresponding to putative sites of pinned TCRs. (D) The UtrCH/actin ratio is high at sites displaying actin enrichment, indicating a primarily stable actin fraction in these regions (1) compared to nearby background areas (2). (Scale bars: 5 μ m.)

Our results show that the T-cell periphery is relatively enriched in mKate2- β -actin (Fig. 1 C, box 1), while EGFP-UtrCH dominates towards the center of the IS (Fig.

1 C, box 2). We infer from this probe distribution that the cytoskeleton at the T-cell periphery is composed of short fragments and is a site of active polymerization, whereas at the center of the IS, actin filaments are longer and predominantly stable. This is consistent with previous models of the T-cell actin

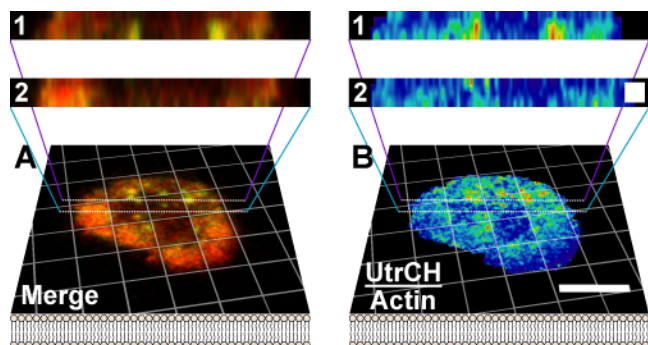


Figure 3. Three-dimensional ratiometric imaging shows that actin enrichment extends away from the cell membrane. Single planes from (A) merged mKate2- β -actin and EGFP-UtrCH and (B) UtrCH/actin ratio three-dimensional stacks show actin enrichment at the cell membrane. Cutouts represent Z-projections passing through sites of enrichment (1) and nearby background regions (2). The color distribution in B is analogous to that in Figs. 1 D and 2 D, and is omitted for clarity. (Scale bar: 5 μ m in the x axis only. Scale box: 1 μ m.)

We limit quantitative analysis of the ratio to its spatial gradients at a single time point, but such analysis is possible in systems that permit rigorous calibration for probe expression and photobleaching.

Actin enrichment at trapped TCR clusters incorporates both mKate2- β -actin (Fig. 2, A and C) and EGFP-UtrCH (Fig. 2, B and C). The relative UtrCH/actin ratio at these sites (Fig. 2 D, box 2) is quite high relative to nearby background areas (Fig. 2 D, box 1), indicating that the actin is derived primarily from the stable actin population.

The three dimensional distribution of TCR-associated actin was analyzed in dual-labeled live T cells using a spinning disk confocal microscope. The recordings show actin extending away from the cell membrane in the vicinity of trapped TCRs, while the rest of the actin cytoskeleton remains relatively flat (Figs. 3 and S1 in the Supporting Material). These

protrusions of actin away from the membrane surface are predominantly composed of stable, filamentous actin, as indicated by their relatively high UtrCH/actin ratio (Fig. 3 B).

Our interpretation of these results is that the filamentous actin network is relatively dense at sites of pinned TCRs. This is the simplest explanation out of several possibilities, one of which is formin-mediated mKate2- β -actin-deficient actin nucleation (17). Filament bunching at pinned TCRs can arise from consistent biophysical properties without assuming heterogeneity between the biochemistry of these receptors and other actin-associated proteins such as those at the cell edge, where locally high probe ratios are absent.

Although TCRs are intentionally trapped as part of this experimental strategy, it is likely APCs can naturally impede TCR ligand mobilities under certain circumstances, and this been shown to impact T-cell signaling (18, 19). Actin architecture near cell surface proteins has been extensively studied in focal adhesions of fibroblasts (20), but the lack of stress fibers in T cells makes it unlikely that the two structures are similar. Thus, receptor-induced cytoskeletal enrichment at TCR clusters adds to the catalog of actin behaviors *in situ*, which is conveniently probed by techniques such as ratiometric dual-probe imaging in live cells. These techniques can be coupled to various spatial analysis algorithms to further extend their utility.

ACKNOWLEDGEMENTS

We thank R. Petit and the Molecular Foundry, Lawrence Berkeley National Laboratory (LBNL) for substrate nanofabrication and S. Lord for assistance with microscopy and assembly of the Supporting Material. We also thank N. Fay and N. Hartman for preparation of key reagents and A. Greene for assistance with microscopy. This work was supported by the Director, Office of Science, Office of Basic Energy Sciences, of the U.S. Department of Energy under contract no. DE-AC02-05CH11231.

REFERENCES AND FOOTNOTES

1. Ryser, J., E. Rungger-Brandle, ..., P. Vassalli. 1982. The area of attachment of cytotoxic T lymphocytes to their target cells shows high motility and polarization of actin, but not myosin. *J. Immunol.* 128: 1159–1162.
2. Bunnell, S.C., V. Kapoor, ..., L.E. Samelson. 2001. Dynamic Actin Polymerization Drives T Cell Receptor-Induced Spreading. *Immunity.* 14: 315–329.
3. Kaizuka, Y., A.D. Douglass, ..., R.D. Vale. 2007. Mechanisms for segregating T cell receptor and adhesion molecules during immunological synapse formation in Jurkat T cells. *Proc. Natl. Acad. Sci. U.S.A.* 104: 20296–20301.
4. Beemiller, P., and M.F. Krummel. 2010. Mediation of T-Cell Activation by Actin Meshworks. *Cold Spring Harb. Perspect. Biol.* 2: a002444.
5. Grakoui, A., S.K. Bromley, ..., M.L. Dustin. 1999. The Immunological Synapse: A Molecular Machine Controlling T Cell Activation. *Science.* 285: 221–227.
6. Dustin, M.L., and J.T. Groves. 2012. Receptor Signaling Clusters in the Immune Synapse. *Annu. Rev. Biophys.* 41: 543–556.
7. Yu, Y., A.A. Smoligovets, and J.T. Groves. 2013. Modulation of T cell signaling by the actin cytoskeleton. *J. Cell Sci.* 126: 1049–1058.

8. Campi, G., R. Varma, and M.L. Dustin. 2005. Actin and agonist MHC-peptide complex-dependent T cell receptor microclusters as scaffolds for signaling. *J. Exp. Med.* 202: 1031–1036.
9. Varma, R., G. Campi, ..., M.L. Dustin. 2006. T Cell Receptor-Proximal Signals Are Sustained in Peripheral Microclusters and Terminated in the Central Supramolecular Activation Cluster. *Immunity*. 25: 117–127.
10. Yu, C., H. Wu, ..., J.T. Groves. 2010. Altered actin centripetal retrograde flow in physically restricted immunological synapses. *PLoS ONE*. 5: e11878.
11. Smoligovets, A.A., A.W. Smith, ..., J.T. Groves. 2012. Characterization of dynamic actin associations with T-cell receptor microclusters in primary T cells. *J. Cell Sci.* 125: 735–742.
12. Gomez, T.S., and D.D. Billadeau. 2008. T Cell Activation and the Cytoskeleton: You Can't Have One Without the Other. *Adv. Immunol.* 97: 1–64.
13. Burkel, B.M., G. von Dassow, and W.M. Bement. 2007. Versatile fluorescent probes for actin filaments based on the actin-binding domain of utrophin. *Cell Motil. Cytoskeleton*. 64: 822–832.
14. Groves, J.T., N. Ulman, and S.G. Boxer. 1997. Micropatterning Fluid Lipid Bilayers on Solid Supports. *Science*. 275: 651–653.
15. Mossman, K.D., G. Campi, ..., M.L. Dustin. 2005. Altered TCR signaling from geometrically repatterned immunological synapses. *Science*. 310: 1191–1193.
16. Yi, J., X.S. Wu, ..., J.A. Hammer. 2012. Actin Retrograde Flow and Acto-Myosin II Arc Contraction Drive Receptor Cluster Dynamics at the Immunological Synapse in Jurkat T-Cells. *Mol. Biol. Cell*. 23: 834–852.
17. Wu, J.-Q., V. Sirotkin, ..., T.D. Pollard. 2006. Assembly of the cytokinetic contractile ring from a broad band of nodes in fission yeast. *J. Cell Biol.* 174: 391–402.
18. Al-Alwan, M.M., G. Rowden, ..., K.A. West. 2001. The Dendritic Cell Cytoskeleton Is Critical for the Formation of the Immunological Synapse. *J. Immunol.* 166: 1452–1456.
19. Hsu, C.-J., W.-T. Hsieh, ..., T. Baumgart. 2012. Ligand Mobility Modulates Immunological Synapse Formation and T Cell Activation. *PLoS ONE*. 7: e32398.
20. Patla, I., T. Volberg, ..., O. Medalia. 2010. Dissecting the molecular architecture of integrin adhesion sites by cryo-electron tomography. *Nat. Cell Biol.* 12: 909–915.

This document was prepared as an account of work sponsored by the United States Government. While this document is believed to contain correct information, neither the United States Government nor any agency thereof, nor the Regents of the University of California, nor any of their employees, makes any warranty, express or implied, or assumes any legal responsibility for the accuracy, completeness, or usefulness of any information, apparatus, product, or process disclosed, or represents that its use would not infringe privately owned rights. Reference herein to any specific commercial product, process, or service by its trade name, trademark, manufacturer, or otherwise, does not necessarily constitute or imply its endorsement, recommendation, or favoring by the United States Government or any agency thereof, or the Regents of the University of California. The views and opinions of authors expressed herein do not necessarily state or reflect those of the United States Government or any agency thereof or the Regents of the University of California.

This manuscript has been authored by an author at Lawrence Berkeley National Laboratory under Contract No. DE-AC02-05CH11231 with the U.S. Department of Energy. The U.S. Government retains, and the publisher, by accepting the article for publication, acknowledges, that the U.S. Government retains a non-exclusive, paid-up, irrevocable, world-wide license to publish or reproduce the published form of this manuscript, or allow others to do so, for U.S. Government purposes.